Enhanced DTI tracking with Adaptive Tensor Interpolation

Alessandro Crippa, Andrei C. Jalba and Jos B. T. M. Roerdink

Abstract A novel tensor interpolation method is introduced that allows Diffusion Tensor Imaging (DTI) streamlining to overcome low-anisotropy regions and permits branching of trajectories using information gathered from the neighbourhood of low-anisotropy voxels met during the tracking. The interpolation method is performed in *Log-Euclidean space* and collects directional information in a spherical neighbourhood of the voxel in order to reconstruct a tensor with a higher linear diffusion coefficient than the original. The weight of the contribution of a certain neighbouring voxel is proportional to its linear diffusion coefficient and inversely proportional to a power of the spatial Euclidean distance between the two voxels. This inverse power law provides our method with robustness against noise. In order to resolve multiple fiber orientations, we divide the neighbourhood of a low-anisotropy voxel in sectors, and compute an interpolated tensor in each sector. The tracking then continues along the main eigenvector of the reconstructed tensors.

We test our method on artificial, phantom and brain data, and compare it with (i) standard streamline tracking, (ii) the Tensorlines method, (iii) streamline tracking after an interpolation method based on bilateral filtering, and (iv) streamline tracking using moving least square regularisation. It is shown that the new method compares favourably with these methods in artificial datasets. The proposed approach gives the possibility to explore a DTI dataset to locate singularities as well as to enhance deterministic tractography techniques. In this way it allows to immediately obtain results more similar to those provided by more powerful but computationally much more demanding methods that are intrinsically able to solve crossing fibers, such as probabilistic tracking or high angular resolution diffusion imaging.

Alessandro Crippa and Jos B. T. M. Roerdink

Johann Bernoulli Institute for Mathematics and Computer Science, University of Groningen, P.O. Box 407, 9700 AK Groningen, The Netherlands, e-mail: `a.crippa@rug.nl`, `j.b.t.m.roerdink@rug.nl`

Andrei C. Jalba

Institute for Mathematics and Computing Science, Eindhoven University of Technology, P.O. Box 513, 5600 MB, The Netherlands, e-mail: `a.c.jalba@tue.nl`

1 Introduction

Diffusion Tensor Imaging (DTI) is a Magnetic Resonance (MR) technique that allows quantitative measurement of three-dimensional diffusion of water molecules in biological tissues [5, 35]. DTI has found many applications in medicine and neuroscience [25, 45] and nowadays is the only method enabling *in vivo* and non-invasive exploration of architectonic organisation of human brain (among other organs), particularly of the cerebral white matter. Self-diffusion of water molecules in white matter is more probable to occur along neural fibers than perpendicular to them [8], leading to anisotropic diffusion of water which reflects the fibrous structure and the directional arrangements of bundles of axons [7]. Although axon myelination seems not to be essential for diffusion anisotropy [52], it is widely assumed to be the major barrier to water diffusion in brain white matter.

The DTI method approximates the diffusion process in each voxel of a DTI dataset by modelling the probability density function of water displacement via a second order diffusion tensor that represents the covariance matrix of a Gaussian diffusion process. This tensor is expressed as a three-by-three symmetric non-negative definite matrix. For each voxel, the tensor's eigensystem is used to describe the local diffusion process; in particular, the principal eigenvector (corresponding to the largest eigenvalue) shows the direction of main diffusivity.

DTI provides an estimation of anatomical connectivity patterns and reconstructs fiber pathways within the human brain [35]. Several techniques have been proposed in the literature: deterministic tractography (or fiber tracking) [4, 14, 24, 30] is one of the most commonly used techniques and relies on the assumption that the principal eigenvector of a tensor accurately describes the orientation of the underlying fiber bundles. This information is used to perform streamlining (or other line propagation techniques) in the vector field induced by the principal eigenvectors of all voxels in the dataset. Fiber tracking has been shown to be effective in many brain regions.

A major limitation of DTI is the fact that local diffusion information is not always sufficient to determine the underlying fiber direction. In the case of low anisotropy, i.e., when the two biggest eigenvalues (or even all three) have comparable magnitude, the principal eigenvector of the tensor does not necessarily correspond to the main diffusion direction. In this case a tensor representation can sometimes provide an approximated average of the multiple compartments present within a voxel [51] and thus the streamlining may suffer from cumulative tracking errors that could lead to erroneous results [28, 41].

Fractional anisotropy (FA) is a measure of the anisotropy of a tensor. Voxels with a small FA mainly occur because of partial volume effects at locations where fiber crossing, fiber branching, or fiber kissing occur when two fibers meet and depart from each other within a voxel [1, 22] (cf. Fig. 1). The presence of low-anisotropy voxels is also related to the resolution of DTI data (being roughly $2 \times 2 \times 2$ mm^3, while axons have a diameter in the order of μm) and to the high susceptibility of DTI to noise during data acquisition [35, 37]. The inability to deal with areas of low anisotropy and to distinguish among singularities (i.e., crossing, branching, or kissing fibers) is considered to be the biggest problem of DTI [6, 30, 46]. Thus a ten-

sor representation may not always be adequate to describe the underlying white matter structure. Possible solutions are to perform MR acquisition with a large number of gradient directions, as in High Angular Resolution Diffusion Imaging (HARDI) [44] or Q-ball imaging [43], or process the data using probabilistic tractography with multiple fiber orientations [9]. However, these methods require longer scanning times and longer preprocessing steps (computing the directional probability distributions needed for probabilistic tractography is very time consuming) and are not always available in current clinical environments.

The method proposed in this paper aims to improve deterministic DTI tracking by adding the ability to solve singularities without introducing a different diffusion model. We present a tensor interpolation method which can achieve noise reduction and resolve singularities to enhance subsequent streamline tractography in areas of low anisotropy. The method improves deterministic fiber tracking by interpolating voxels with low anisotropy reached during the tracking process. In such voxels directional information is gathered from the neighbourhood and the track is split to follow both crossing or kissing fibers. Our approach provides a good alternative when more involved approaches are not available or when the emphasis is more on speed than quality: while probabilistic tractography requires hours of preprocessing, our method detects and resolves fiber crossings in a few seconds.

2 Related Work

The issue of characterising fiber orientation in voxels with a population of more than one fiber has been addressed in several ways in the literature [23]. Model-based approaches include for instance multiple tensor fitting [11, 40, 44], probabilistic techniques [9, 10, 27, 29, 31], DTI tracking based on front propagation algorithms [32, 33, 38], and higher order tensor models [20]. Model free approaches include Diffusion Spectrum Imaging (DSI) [47], HARDI [44] and Q-ball Imaging [43]. For a review of tracking methods we refer to [2].

The importance of considering singularities in fiber tracking algorithms has been shown by Behrens *et al.* [9]. Nevertheless, depending on the quality of the data and the complexity of the tissue, model parsimony measures are required to determine when more complex models are justified [23]. For instance, probabilistic and front propagation algorithms can intrinsically resolve singularities but have the major drawback not to output a connection path but values describing the likelihood to find a connection between two brain regions. Hence the user has to heuristically set a threshold on these values and decide how reliable the result is.

The method proposed in this paper has been inspired by three different papers: Hamarneh & Hradsky's bilateral filtering of tensors [19], the surface reconstruction method via Coulomb potentials [21], and the Tensorlines propagation method by Weinstein *et al.* [48]. Bilateral filtering of DTI data is a technique that tries to reduce noise by identifying and delineating areas with similar diffusion properties. Several papers on interpolation of tensor data or of expressions derived from tensors

(such as eigenvalues, eigenvectors, or FA) have been published [16, 18, 36, 42]. For instance, Westin and Knutson [50] have shown how normalised convolution can be used as regularisation of tensor fields. Welk *et al.* [49] proposed median filtering, and Castano-Moraga *et al.* [12] proposed anisotropic interpolation of DT-MRI data. Hamarneh's method is the application of bilateral filtering to DTI images and seems to perform well in detecting edges in tensor fields. It can also handle, as a special case, tensor interpolation; see the Appendix for more information on this method.

The surface reconstruction method proposed in [21] is not related to DTI; it is an approach that tries to gather the necessary information from the whole dataset, weighting the contribution of each sample by its distance from the area to be interpolated. Using the whole dataset instead of only a certain neighbourhood of the surface gives this method a better resistance to noise. We incorporate an adapted version of this distance weighting in our method.

The Tensorlines method [48] does not address the issue of estimating a smooth tensor but it is a technique that adaptively interacts with streamline propagation using the whole local tensor information to deflect the incoming tracking direction. In this method the tracking direction in a voxel is defined by the collinearity between the local main eigenvector and the main eigenvector of the previously visited voxel. This method does not solve singularities but can perform tracking in low-anisotropy regions and can produce longer tracks than standard streamlining. A drawback of this method is that the integration step for tracking the fibers is equal to the voxel size, while standard streamlining usually uses smaller integration steps. Furthermore, this tracking technique seems to be very sensitive both to noise and to the parameters set by the user, who has to choose the relative weight of the incoming direction for the local tracking.

Another interpolation method that adaptively interpolates tensors along streamlines is the technique proposed by Zhukov *et al.* [53]. This method is based on a moving least square regularisation of the tensors along the streamline. After reconstructing a continuous tensor field in the volume through trilinear interpolation, the method finds a polynomial that fits the data, in a least square sense, in a region around the tensor to be interpolated. The fitting depends on the location, the orientation of the streamline at the point, and the history of motion along the streamline. This method was successfully applied to brain as well as heart diffusion data [53, 54].

3 Methods

Our method is meant to enhance deterministic tracking techniques by interpolating diffusion information from neighbourhoods of voxels with low anisotropy. Inspired by [48] and [53], we do not apply interpolation to every voxel of the dataset but only to those voxels reached during tracking. When a voxel with low anisotropy is reached, regional information is gathered from the surrounding voxels and this is used to find the direction, or directions, in which to continue the tracking.

This prevents, in contrast to global interpolation, that the interpolation affects high anisotropy as well as low-anisotropy voxels.

The basic steps of our algorithm are the following:

1. Choose a starting voxel in the dataset and start tracking a fiber.
2. Continue the tracking until a voxel with low FA is reached (FA< 0.3).
3. If such a voxel is encountered, interpolate the neighbouring voxels to find an interpolated tensor with higher FA than the original. If this is possible, continue the tracking along the main eigenvector of this tensor.
4. Visualise the resulting fiber.

3.1 Tensor Interpolation

Diffusion tensors do not form a vector space and special attention must be paid when performing calculations on them [34] (cf. Fig. 6). The value of the determinant of a tensor is in fact a measure of the dispersion of the diffusion process [3] and Euclidean averaging of tensors has been shown to lead tensor swelling effects [13, 17, 42]. This could lead to a decrease of FA and to a possible stopping of the tracking algorithm. Therefore tensor averaging is performed in *Log-Euclidean space* as proposed by Arsigny [3]. Performing computations in this space prevents the increase of the determinant of the averaged tensor [15].

We recall here that the logarithm of a tensor T is defined as

$$\log_m(T) = R^T \log(D) R,$$

where D is the diagonal matrix of the eigenvalues of T and R is the matrix of its eigenvectors. The formula for tensor exponentiation $\exp_m$ is analogous.

Given a (low-anisotropy) voxel at a certain position x, the corresponding tensor $T(x)$ is interpolated by gathering information from a neighbourhood of x containing N voxels. The weight of the contribution of a certain neighbouring voxel at position ξ_i is set proportional to its linear diffusion coefficient $C_L(\xi_i)$ and, like in [21], inversely proportional to a power n of the spatial Euclidean distance between the two voxels x and ξ_i:

$$w(x, \xi_i) = C_L(\xi_i) d(x, \xi_i)^{-n} \tag{1}$$

The linear diffusion coefficient C_L is a rotational invariant of a diffusion tensor [26] that measures the amount of linear diffusion in comparison to the overall diffusion. It is defined as

$$C_L = \frac{\lambda_1 - \lambda_2}{\lambda_1 + \lambda_2 + \lambda_3} \tag{2}$$

where $\lambda_1, \lambda_2, \lambda_3$ are the three eigenvalues of the tensor, ordered from the largest to the smallest.

For a low-anisotropy voxel x an interpolated tensor $\tilde{T}(x)$ is thus computed according to the following formula:

$$\tilde{T}(x) = \exp_m \left(k \cdot \log_m(T(x)) + (1-k) \cdot \sum_{i=1}^{N} \frac{w(x, \xi_i)}{W(x)} \log_m(T(\xi_i)) \right) \qquad (3)$$

where

$$W(x) = \sum_{i=1}^{N} w(x, \xi_i) \qquad (4)$$

is the total weight at voxel x. The parameter k weights the influence of the tensor $T(x)$ and the influence of the neighbouring tensors $T(\xi_i)$. It allows us to divide the local and regional information into two complementary components. As explained above, the tensor logarithm and tensor exponentiation used in this equation are obtained by computing the eigenvalues and eigenvectors of the tensor field.

The weighting provided by C_L ensures that voxels with predominantly linear diffusion will provide more information than voxels with planar or isotropic diffusion. We prefer to use the linear coefficient instead of the more commonly used FA because we eventually aim to eigensolve the interpolated tensor and find proper directions to follow during tracking. For this reason we want to give the same weight (given equal spatial distance from the voxel to be interpolated) to voxels with planar diffusion and to voxels with isotropic diffusion; using FA would have given more weight to voxels with planar diffusion.

The inverse power law dependence of the weight on the distance extends the area of influence so that even voxels further away will contribute to the interpolation. This approach allows us, by taking the exponent $n > 1$, to consider a wider area of influence than using a weighting that is linearly proportional to the inverse of the distance. As shown in [21], this provides our method with more robustness against noise. In contrast to the approach of [21], we do not extend the radius of influence to the whole dataset, which would not be physically plausible for DTI brain data, but restrict it to a spherical neighbourhood of the voxel under consideration. In the artificial dataset of Fig. 3, where the low FA area is very large, a neighbourhood of 10 voxels was used for tracking; a neighbourhood of only 5 voxels was used for the tracking in the synthetic volume and in the brain volume.

3.2 Extended DTI model

Because low-anisotropy voxels are mainly due to partial volume effects, the tensor model cannot distinguish among cases in which crossing, kissing or branching fibers occur within a single voxel (cf. Fig. 1). Thus, interpolation techniques may fail or lead to erroneous results and it is not possible to tell if the tracking is following the correct direction once it encounters a low FA voxel.

The second ingredient of our approach is meant to tackle this problem as follows. Whenever the tracking enters a low anisotropy voxel x, its 3D neighbourhood is divided in 26 sectors S_i, one per direct neighbour (on the voxel grid, using 26-connectivity). An interpolated tensor $\tilde{T}_i(x)$ is computed for each sector S_i,
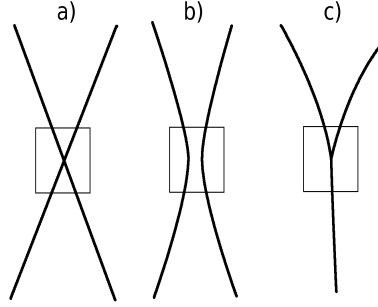
Fig. 1 Schematics of possible scenarios in a local fiber configuration. Within a voxel the fibers can (a) cross each other, (b) kiss each other or (c) a fiber can split into two branches.
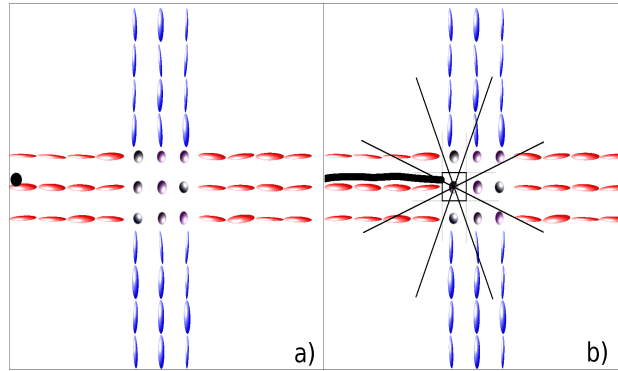

Fig. 2 Dataset subdivision when a low FA voxel is reached by the tracking (2D case; the 3D case is a straightforward extension). a) The figure shows two fibers meeting in the center of an example dataset. Tensors are displayed as ellipsoids whose major axis corresponds to the main eigenvector and whose eccentricity depicts the amount of anisotropy; the colour indicates the direction of main diffusivity (red: horizontal, blue: vertical). A seed is positioned in the black spot. b) When the tracking (black line) reaches a low FA voxel (square) the dataset is uniformly subdivided into eight sectors; each sector is centered at a direct neighbour of the low-FA voxel. Tensors are computed in each slice according to equation Eq. (3).

$i = 1, \ldots, 26$ according to Eq. (3), by interpolating the tensors of sector S_i (cf. Fig. 2). For each sector S_i, centered at a voxel x, a likelihood value $l_i(x)$ is computed by

$$l_i(x) = (\tilde{C}_L^i(x)\mathbf{v}_i(x)) \cdot \mathbf{u}_i \qquad (5)$$

where $\mathbf{v}_i(x)$ is the principal eigenvector of the interpolated tensor $\tilde{T}_i(x)$ and $\mathbf{u}_i$ is the unit vector bisecting sector S_i (here $\mathbf{u} \cdot \mathbf{v}$ denotes the dot product of two vectors $\mathbf{u}$ and $\mathbf{v}$). $\tilde{C}_L^i(x)$ is the average distance-weighted linear diffusion coefficient in sector S_i,

$$\tilde{C}_L^i(x) = \sum_{j \in S_i} C_L(\xi_j) d(x, \xi_j)^{-n}.$$

The values $l_i(x)$ are used as the likelihood for each sector S_i that the tracking should continue along the direction $\mathbf{u}_i(x)$ (cf. Fig. 2). Because of the impossibility of differentiating between crossing, kissing or branching fibers, we continue tracking along the bisections of the two sectors with the highest likelihood value. Sectors whose unit vector forms an angle bigger than 80 degrees with the incoming tracking direction are discarded (according to the literature, a fiber bundle should not bend more than 80 degrees within a single voxel). Doing so we both spot the singularity and continue tracking along the correct direction.

Although it would in principle be possible to follow more directions, we chose to continue the tracking only along two directions, resolving in this way the crossing of not more than two fibers. It is not possible to determine the number of fibers that may produce the partial volume effect in a voxel, and two is obviously the lower bound.

4 Results

In this section we present results of our method for artificial data, phantom data and DTI brain scans; the method is also compared with existing techniques.

4.1 Artificial data

4.1.1 High anisotropy area with a low-anisotropy core

The first artificial dataset we used consists of a $20 \times 20 \times 20$ three-dimensional tensor field containing high-anisotropy voxels (FA = 0.85) but with a cubic ($7 \times 7 \times 7$ voxels) low-anisotropy core (FA = 0.1), cf. Fig. 3, left upper picture. Tensors in the high-anisotropy area are aligned to the vertical direction, while tensors in the low-anisotropy area are aligned to the horizontal direction. This dataset is used to compare our method (streamline tracking combined with the new interpolation method) with (i) standard streamline tracking, (ii) the Tensorlines method, (iii) streamline tracking after an interpolation based on bilateral filtering of tensors (see the Appendix) and (iv) streamline tracking using moving least square regularisation. The tests conducted on this dataset explore the ability of the different approaches to reconstruct fibers passing through the low-anisotropy area.

White Gaussian noise was added to each tensor component. Figure 3 shows the central slice of the dataset and a comparison among standard streamline tracking, Tensorlines and our new method. Deterministic tractography was achieved using Euler integration. The top right figure shows that standard tracking stops as soon as it reaches the low-FA area. Tensorlines tracking (bottom left) gets distorted already

with a low noise level ($\sigma = 0.02$), while our method (bottom right) is able to reconstruct the connection between the upper part and the lower part of the dataset. For illustration purposes, the interpolation was applied to the whole dataset (and not only to the voxels reached by the tracking) to show its effects on directionality and on FA values.
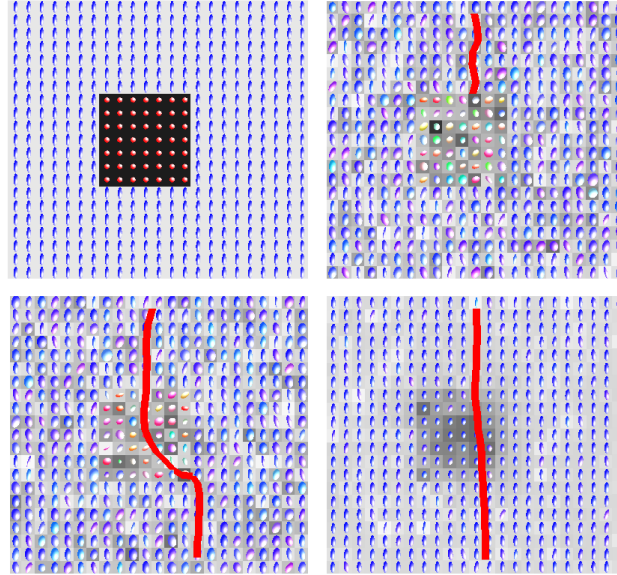

Fig. 3 Top left: the artificial dataset is a $20{\times}20{\times}20$ three-dimensional tensor field consisting of highly anisotropic tensors (FA= 0.85) with a $7{\times}7{\times}7$ low-anisotropy area (FA=0.1) in the middle. The picture shows the central slice of the dataset. Background colour represents FA (black: 0, white: 1); the colour of the ellipsoids represents direction (blue: vertical, red: horizontal). Top right: white Gaussian noise ($\sigma = 0.02$) was added to each tensor component. Streamline tracking (red line) was seeded in a single voxel in the top of the picture. Bottom left: the Tensorlines technique. Bottom right: streamline tracking after our new tensor interpolation.

Figure 4 shows a comparison among our method, interpolation based on bilateral filtering, and Zhukhov's moving least square regularisation. Since these methods were all able to track through the low-anisotropy region of Fig. 3, we measured the effectiveness of the three interpolation techniques on three different voxels in the dataset: the voxel in the middle of the low-anisotropy area; a voxel with low FA, directly on the border of the inner low-FA core, and a high-FA voxel on the border of the inner core. Three different measures were used to compare the techniques. First, the FA value of the interpolated voxel; this shows the ability of each technique to gather anisotropy from the neighbourhood. Second, the Log-Euclidean distance between the interpolated voxel and a voxel in the high-FA area (before the noise addition); this indicates the ability to reconstruct the tensors. Third, the angular difference, in degrees, between the main eigenvector of the reconstructed tensor

and the main eigenvector of a voxel in the high-FA area (before the noise addition); this indicates the ability to perform correct tracking after interpolation.

The experiments were conducted at several noise levels. Gaussian white noise was added individually to each tensor component with standard deviation σ varying between 0.001 and 0.025. For each noise level we repeated the experiment 25 times. When adding Gaussian noise, we maintained the non-negative definiteness of the diffusion tensor. This prevents to generate tensors with non positive eigenvalues which are difficult to interpret physically (since they describe non positive diffusion factors) [3].

As seen in Fig. 4, the interpolated tensors present an FA always bigger than 0.3, even at relatively high noise levels (a threshold of FA = 0.2 is usually used as a stopping criterion for streamline tractography). Our method is more effective in restoring high-FA values than the interpolation based on bilateral filtering, and it is also more effective than moving least square regularisation, except for high noise levels. The Log-Euclidean distance between the interpolated tensors and the "expected" tensor is quite small in all three cases. Again, our results show lower Log-Euclidean distances than those achieved by the interpolation based on bilateral filtering, except for a small region below $\sigma = 0.02$ in Fig. 4(f). Compared with moving least square regularisation, our method produces lower Log-Euclidean distances especially for the voxel the center of the low FA region (Fig. 4(d)). Regarding the angular error of the three interpolation techniques we see no significant difference, see Fig. 4(g, h, i). The average angular error grows roughly linearly with the amount of noise, and it does not exceed 6 degrees (at $\sigma = 0.025$).

4.1.2 Crossing fibers

The second artificial dataset consisted of three fibers that meet each other in the center of a $20 \times 20 \times 20$ dataset. Each fiber is represented by a strip of high-FA voxels (FA = 0.85). The dataset was used to evaluate the ability of our method to recognise directional information in different sectors of the dataset. Figure 5(left) shows a slice of the dataset where the three fibers cross. Tracking was seeded at the top of the figure and the track did split when it reached the low-FA area. White Gaussian noise was added to each tensor of the dataset and the tracking was repeated 25 times per noise level; the standard deviation of the noise varied from 0.001 to 0.25. Figure 5(right) shows statistics on the ability to find the correct fibers as a function of noise level. The blue line represents the probability to find all five segments that meet in the low-FA area (the incoming direction was not considered as a possible solution). The blue shaded area represents its standard deviation. The red line indicates the probability to find the two fibers that the algorithm should detect, i.e., the only two fibers forming an angle smaller than 80 degrees with the incoming direction. The red shaded area is its standard deviation.
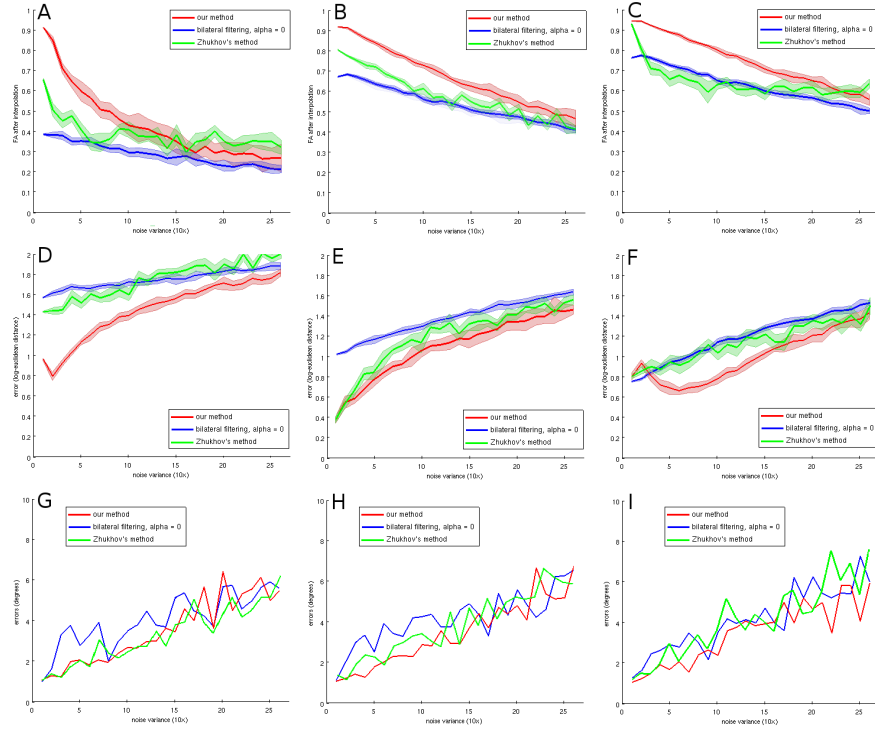
Fig. 4 Comparison between results achieved by our method (red lines), by the interpolation based on bilateral filtering (blue lines), and by the moving least square regularisation method of Zhukov *et al.* (green lines). Error measures were computed for three different voxels in the dataset shown in Fig. 3: a voxel in the middle of the low-anisotropy area (column 1), a voxel with low FA, directly on the border of the inner low-FA core (column 2), and a high-FA voxel on the border of the inner core (column 3). Row 1: FA value of the interpolated voxel. Row 2: Log-Euclidean distance between the interpolated voxel and a voxel in the high-FA area. Row 3: angular error of the interpolated voxel. All error measures are shown as a function of noise level σ. Each line represents the average of 25 runs and the shaded area indicates the corresponding standard deviation.

4.2 Phantom data

The next dataset considered was a physical phantom DTI dataset representing two 90 deg crossing fibers. The dataset was made of Dyneema® fibers. The fibres were grouped in parallel bundles of 780 filaments which were crossed, surrounded by a shrinking tube, and immersed in water (Courtesy of E. Fieremans, NYU Medical Center, and J. Sijbers, Univ. of Antwerp). Figure 7 shows a comparison among standard deterministic tractography, our method and the results of probabilistic tracking performed with FSL [39]. The white disc indicates the position where the tracking was seeded. No constraints were set on the angles between the incoming and the outgoing directions. Standard deterministic tractography was not able to resolve the
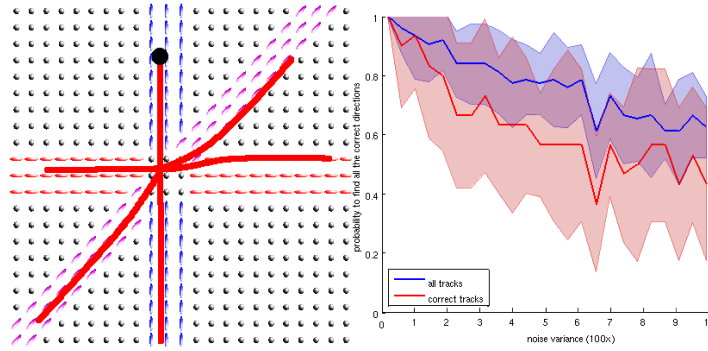
Fig. 5 Left: artificial dataset with three fibers crossing in the middle. The figure shows the central slice of the dataset. Tracking was seeded in the black spot. The tracking follows the fiber until the low-anisotropy area in the middle and then detects all other fibers. Right: The blue line shows the probability, as a function of noise level, to detect all five fibers meeting in the center (the incoming direction was not considered as a solution). The red line indicates the probability to find the two fibers that the algorithm should detect (the only two fibers forming an angle smaller than 80 degrees with the incoming direction).

crossing: the tracking stopped when it encountered a low FA voxel. Our algorithm (which is deterministic as well) recognised all the fiber segments and it was able to continue tracking in all the directions detected by the much more computationally demanding probabilistic method.
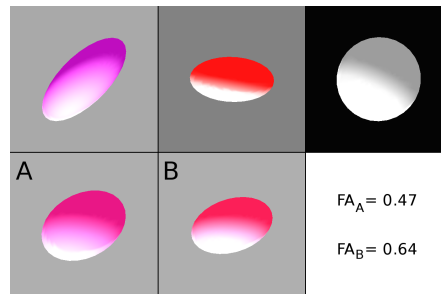

Fig. 6 Comparison between averaging of tensors in Euclidean versus Log-Euclidean space. First row: three input tensors. Second row: tensor A is obtained by Euclidean averaging, tensor B by log-Euclidean averaging. The tensor in A shows a lower FA compared to the tensor in B.
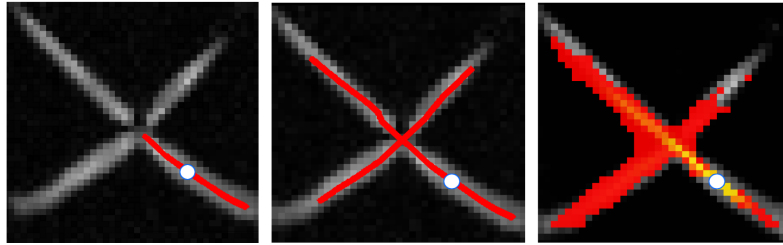
Fig. 7 Tracking performed in a physical phantom DTI dataset depicting two crossing fibers. The pictures show a slice of the dataset. The white disc indicates the position where the tracking was seeded. Left: tracking results of standard deterministic tractography; the tracking stopped in the crossing area. Middle: results of our algorithm; crossing fibers were detected and all branches were found. Right: tracking by probabilistic tractography with FSL.
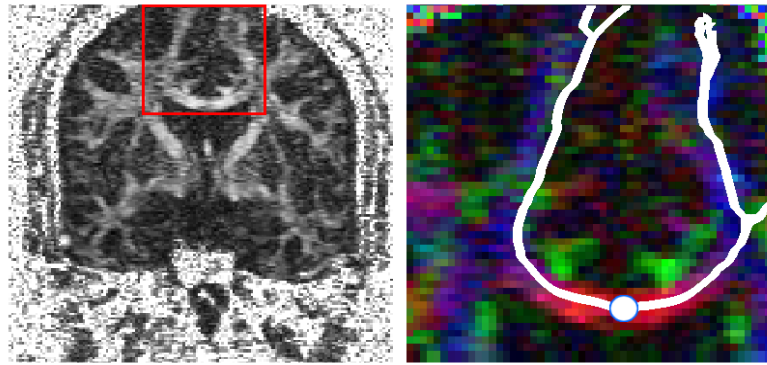

Fig. 8 Tracking performed for a DTI brain dataset. The red square in the left picture indicates the Corpus Callosum. The right picture shows a magnification of the red area. The white disc indicates the position where tracking was seeded. Our algorithm was able to detect the blossoming of the fibers of the Corpus Callosum below the cerebral cortex (leftmost branch) and the intersection between Corpus Callosum and Corona Radiata (rightmost branch).

4.3 Brain data

Results of the tracking for a DTI brain data set are shown in Fig. 8. A coronal slice of the brain is shown in the leftmost figure, colour coded according to the FA values (black represents FA=0 and white FA=1). Seeding the tracking in the lower part of the body of the Corpus Callosum, our method was able to detect the blossoming of the upper part of the Corpus Callosum where the fibers reach the cerebral cortex, and to resolve the low-FA area generated by the intersection of Corpus Callosum and Corona Radiata. Brain dataset courtesy of Gordon Kindlmann, Scientific Computing and Imaging Institute, University of Utah, and Andrew Alexander, W. M. Keck

Laboratory for Functional Brain Imaging and Behavior, University of Wisconsin-Madison.

5 Conclusions

DTI tractography allows the inference of connectivity patterns within white matter of the brain. There are two main limitations of this technique. The first is that the tensor model does not always reflect the underlying white matter structure, as it is not able to deal with singularities such as crossing, branching, or kissing fibers. The second limitation is the inability of DTI tracking to reconstruct more than one trajectory per seed point.

In this paper we introduced an improved tracking technique that allows DTI streamlining to solve low-anisotropy regions and permits branching of trajectories. Our method performs interpolation for any low-anisotropy voxel met during tracking. Interpolation is computed in *Log-Euclidean space* [3] and collects directional information in a spherical neighbourhood of the voxel in order to reconstruct a tensor with a higher linear diffusion coefficient than the original. The weight of the contribution of a certain neighbouring voxel is proportional to its linear diffusion coefficient and inversely proportional to a power of the spatial Euclidean distance between the two voxels. This inverse power law provides our method with robustness against noise [21] . In order to resolve multiple fiber orientations, we divide the neighbourhood of the low-anisotropy voxel in 26 sectors, and compute an interpolated tensor in each sector according to the weighted tensor interpolation formula. The tracking then continues along the main eigenvector of the reconstructed tensor.

We tested our method on artificial, phantom and brain data, and compared with existing methods: (i) standard streamline tracking, (ii) the Tensorlines method, (iii) streamline tracking after an interpolation based on bilateral filtering, and (iv) moving least square regularisation. We showed that in contrast to standard streamline tracking, our method is able to continue tracking in low-anisotropy areas, while Tensorlines tracking gets distorted already for low noise levels. Compared to streamline tracking after the interpolation based on bilateral filtering, our method is more effective in restoring high anisotropy values. Compared to the moving least square regularisation, our method generally performed better except for high noise levels. For phantom and real MRI data, we found that our method was able to detect the same tracts as probabilistic tracking.

Due to its ability to resolve cases of multiple fiber orientations in a single voxel our method gives the possibility to obtain, in comparison to standard deterministic tractography, results more similar to those provided by more powerful techniques that are intrinsically able to solve crossing fibers, such as high angular resolution diffusion imaging, which is not always available, or probabilistic tracking with multiple fiber orientations [39], which is computationally much more demanding: while probabilistic tractography requires hours of preprocessing, our method detects and resolves the crossing in a few seconds. Furthermore, in contrast to the probabilistic

tractography, in our approach there is no need to perform heuristic thresholding for interpreting the results.

Future work will include a deeper study on the results achievable with this method in comparison with probabilistic tracking and other techniques that allow multiple fiber orientations per voxel. Validation of the results, e.g., by histological analysis, will certainly be a requirement for the practical application of this and other DTI techniques.

6 Acknowledgements

7 Appendix

Bilateral filtering of diffusion tensor data is achieved according to the following formula [19]:

$$T(x) = exp_m \left(\sum_{i=1}^{N} \frac{w_i(x)}{k(x)} log_m(T(\xi_i)) \right) \tag{6}$$

$$w_i(x) = \alpha f_1(d_T(T(x), T(\xi_i)) + (1-\alpha) f_2(d_S(x, \xi_i)) \tag{7}$$

where $d_T(T(x), T(\xi_i))$ is the tensor dissimilarity between the two tensors $T(x)$ and $T(\xi_i)$. $d_S(x, \xi_i)$ is the spatial Euclidean distance between the voxels x and ξ_i. Here f_1 and f_2 are monotonically decreasing functions that map d_T and d_S in the interval $[0, 1]$. The value α weights the contribution of the two distances. We used a simplified version of bilateral filtering, by setting α to zero and thus weighting the contribution of the tensor $T(\xi_i)$ only according to the Euclidean distance between voxels x and ξ_i.

References

1. Alexander, A.: Analysis of partial volume effects in diffusion tensor MRI. Magn. Reson. Med. **45**(5), 770–780 (2001)
2. Alexander, D.C.: Multiple-fiber reconstruction algorithms for diffusion MRI. Annals N Y Acad Sci **1064**, 113–133 (2005)
3. Arsigny, V., Fillard, P., Pennec, X., Ayache, N.: Log-Euclidean metrics for fast and simple calculus on diffusion tensors. Magn. Reson. Med. **56**(2), 411–421 (2006)
4. Bammer, R., Acar, B., Moseley, M.E.: In vivo MR tractography using diffusion imaging. Eur. J. Radiol. **45**(3), 223–234 (2003)
5. Basser, P.J., Mattiello, J., Bihan, D.L.: Estimation of the effective self-diffusion tensor from the NMR spin-echo. J. Magn. Reson. **103**(3), 247–254 (1994)

6. Basser, P.J., Pajevic, S., Pierpaoli, C., Duda, J., Aldroubi, A.: In vivo fiber tractography using DT-MRI data. Magn. Reson. Med. **44**(4), 625–632 (2000)
7. Basser, P.J., Pierpaoli, C.: Microstructural and physiological features of tissues elucidated by quantitative-diffusion-tensor MRI. J. Magn. Reson. **111**(3), 209–219 (1996)
8. Beaulieu, C.: The basis of anisotropic water diffusion in the nervous system - a technical review. Nucl. Magn. Res. in Biomed. **15**(7-8), 435–455 (2002)
9. Behrens, T., Johansen-Berg, H., Jabdi, S., Rushworth, M.F., Woolrich, M.W.: Probabilistic diffusion tractography with multiple fibre orientations: What can we gain? Neuroimage **34**(1), 144–155 (2007)
10. Behrens, T.E.J., Woolrich, M.W., Jenkinson, M., Johansen-Berg, H., Nunes, R.G., Clare, S., Matthews, P.M., Brady, J.M., Smith, S.M.: Characterization and propagation of uncertainty in diffusion-weighted MR imaging. Magn. Reson. in Medicine **50**(5), 1077–1088 (2003)
11. Bergmann, O., Kindlmann, G., Peled, S., Westin, C.F.: Two-tensor fiber tractography. In: Proc. ISBI, pp. 796–799 (2007)
12. Castano-Moraga, C., Rodrigues-Florido, M.A., Alvarez, L., Westin, C.F., Ruiz-Alzola, J.: Anisotropic interpolation of DT-MRI data. In: Proc. MICCAI, pp. 343–350 (2004)
13. Chefd'hotel, C., Tschumperlé, D., Deriche, R., Faugeras, O.: Regularizing flows for constrained matrix-valued images. J. Math. Imaging Vision **20**(1-2), 147–162 (2004). DOI http://dx.doi.org/10.1023/B:JMIV.0000011324.14508.fb
14. Conturo, T.E., Lori, N.F., Cull, T.S., Akbudak, E., Snyder, A.Z., Shimony, J.S., McKinstry, R.C., Burton, H., Raichle, M.E.: Tracking neuronal fiber pathways in the living human brain. Proc. Natl. Acad. Sci. USA **96**(18), 10,422–10,427 (1999)
15. Corouge, I., Fletcher, P., Joshi, S., Gouttard, S., Gerig, G.: Fiber tract-oriented statistics for quantitative diffusion tensor MRI analysis. Med. Image Anal. **10**(5), 786–798 (2006)
16. Coulon, O., Alexander, D.C., Arridge, S.A.: A regularization scheme for diffusion tensor magnetic resonance images. In: Proc. of the 17th Int. Conf. Inf. Proc. Med. Imag., vol. 2082, pp. 92–105 (2001)
17. Feddern, C., Weickert, J., Burgeth, B., Welk, M.: Curvature-driven PDE methods for matrix-valued images. Int. J. Comput. Vision **69**(1), 93–107 (2006). DOI http://dx.doi.org/10.1007/s11263-006-6854-8
18. Hahn, K., Pigarin, S., Putz, B.: Edge preserving regularization and tracking for diffusion tensor imaging. In: MICCAI, vol. 2208, pp. 195–203 (2001)
19. Hamarneh, G., Hradsky, J.: Bilateral filtering of diffusion tensor magnetic resonance images. IEEE Trans Image Process. **16**(10), 2463–2475 (2007)
20. Hlawitschka, M., Scheuermann, G.: HOT- Lines: Tracking lines in higher order tensor fields. In: Proc. IEEE Visualization, pp. 27–34 (2005)
21. Jalba, A., Roerdink, J.B.T.M.: Efficient surface reconstruction using generalized Coulomb potentials. IEEE Trans. Vis. Comput. Graph. **13**(6), 1512–1519 (2007)
22. Jones, D.K.: Determining and visualizing uncertainty in estimates of fiber orientation from diffusion tensor MRI. Magn. Reson. Med. **49**(1), 7–12 (2003)
23. Jones, D.K.: Studying connections in the living human brain with diffusion MRI. Cortex **44**(8), 936–952 (2008)
24. Jones, D.K., Simmons, A., Williams, S.C.R., Horsfield, M.A.: Non-invasive assessment of axonal fiber connectivity in the human brain via diffusion tensor MRI. Magn. Res. Med. **42**(1), 37–41 (1999)
25. Kanaan, R.A.A., Kim, J.S., Kaufmann, W.E., Pearlson, G.D., Barker, G.J., McGuire, P.K.: Diffusion tensor imaging in schizophrenia. Bio. Psychiatry **58**(12), 921–929 (2005)
26. Kingsley, P.B.: Introduction to diffusion tensor imaging mathematics: Part I. tensors, rotations, and eigenvectors. Concepts in Magn. Reson **28A**(2), 101–122 (2005)
27. Koch, M.A., Norris, D.G., Hund-Georgiadis, M.: An investigation of functional and anatomical connectivity using magnetic resonance imaging. NeuroImage **16**(1), 241–250 (2002)
28. Lazar, M., Weinstein, D.M., Tsuruda, J.S., Hasan, K.M., Arfanakis, K., Meyerand, M.E., Badie, B., Rowley, H.A., Haughton, V., Field, A., Alexander, L.A.: White matter tractography using diffusion tensor deflection. Human Brain Mapp. **18**(4), 306–321 (2003)

29. McGraw, T., Nadar, M.: Stochastic DT-MRI connectivity mapping on the GPU. IEEE Trans. Vis. Comp. Graphics **13**(6), 1504–1511 (2007)
30. Mori, S., Crain, B.J., Chacko, V.P., vanZijl, P.C.: Three dimensional tracking of axonal projections in the brain by magnetic resonance imaging. Ann. Neurol. **45**(2), 265–269 (1999)
31. Parker, G.J., Haroon, H.A., Wheeler-Kingshott, C.A.: A framework for a streamline-based probabilistic index of connectivity (PICo) using a structural interpretation of MRI diffusion measurements. J Magn Reson Imaging **18**, 242–254 (2003)
32. Parker, G.J.M., Stephan, K.E., Barker, G.J., Rowe, J.B., MacManus, D.G., Wheeler-Kingshott, C.A.M., Ciccarelli, O., Passingham, R.E., Spinks, R.L., Lemon, R.N., Turner, R.: Inizial demonstration of in vivo tracing of axonal projections in the macaque brain and comparison with the human brain using tensor imaging and fast marching tractography. NeuroImage **15**(4), 797–809 (2002)
33. Parker, G.J.M., Wheeler-Kingshott, C.A.M., Barker, G.J.: Estimating distributed anatomical connectivity using fast marching methods and diffusion tensor imaging. IEEE Trans. Med. Imaging **21**(5), 505–51 (2002)
34. Pennec, X., Fillard, P., Ayache, N.: A Riemannian framework for tensor computing. Int. J. Comput. Vis. **66**(1), 41–66 (2004)
35. Pierpaoli, C., Jezzard, P., Basser, P.J., Barnett, A., DiChiro, G.: Diffusion tensor MR imaging of the human brain. Radiology **201**(3), 637–648 (1996)
36. Poupon, C., Mangin, J., Frouin, V., Regis, J., Poupon, F., Pachot-Clouard, M., Bihan, D.L., Bloch, I.: Regularization of MR diffusion tensor maps for tracking brain white matter bundles. In: MICCAI, pp. 489–498 (1998)
37. Poupon, C., Mangin, J.F., Clark, C.A., Frouin, V., Regis, J., Bihan, D.L., Bloch, I.: Towards inference of human brain connectivity from MR diffusion tensor data. Med. Image Anal. **5**(2), 1–15 (2001)
38. Sethian, A.: A fast marching level set method for monotonically advancing fronts. Prod. Natl. Acad. Sci. USA **93**(4), 1591–1955 (1996)
39. Smith, S.M., Jenkinson, M., Woolrich, M.W., Beckmann, C.F., Behrens, T.E., Johansen-Berg, H., Bannister, P.R., Luca, M.D., Drobnjak, I., Flitney, D.E., Niazy, R.K., Saunders, J., Vickers, J., Zhang, Y., Stefano, N.D., Brady, J.M., Matthews, P.M.: Advances in functional and structural MR image analysis and implementation as FSL. NeuroImage **23**(Supplement 1), S208 – S219 (2004). DOI DOI:10.1016/j.neuroimage. 2004.07.051. URL `http://www.sciencedirect.com/science/article/ B6WNP-4DD8GN8-3/2/6ac12c5eb9e31a1b5b3d32324c144489`. Mathematics in Brain Imaging
40. Sotiropoulos, S., Bai, L., Morgan, P.S., Auer, D.P., Constantinescu, C.S., Tench, C.R.: A regularized two-tensor model fit to low angular resolution diffusion images using basis directions. J. Magn. Reson. Imag. **28**(1), 199–209 (2008)
41. Staempfli, P., Jaermann, T., Crelier, G.R., Kollias, S., Valavanis, A., Boesiger, P.: Resolving fiber crossing using advanced fast marching tractography based on diffusion tensor imaging. NeuroImage **30**(1), 110–120 (2006)
42. Tschumperlé, D., Deriche, R., Deriche, R.: Diffusion tensor regularization with constraints preservation. In: IEEE Computer Society Conference on Computer Vision and Pattern Recognition, vol. 1, pp. 948–953 (2001)
43. Tuch, D.S.: Q-ball imaging. Magn. Reson. Med. **52**(6), 1358–1372 (2004)
44. Tuch, D.S., Reese, T.G., Wiegell, M.R., Makris, N., Belliveau, J.W., Wedeen, V.J.: High angular resolution diffusion imaging reveals intra voxel white matter fiber heterogeneity. Magn. Reson. Med. **48**, 577–582 (2002)
45. Walker, J.C., Guccione, J.M., Jiang, Y., Zhang, P., Wallace, A.W., Hsu, E.W., Ratcliffe, M.B.: Helical myofiber orientation after myocardial infraction and left ventricular surgical restoration in sheep. J. Thoracic Cardiov. Surgery **129**(2), 382–390 (2005)
46. Watts, R., Liston, C., Niogi, S., Ulug, A.M.: Fiber tracking using magnetic resonance diffusion tensor imaging and its applications to human brain development. Ment. Retar. Dev. Disabil. Res. Rev. **9**(3), 168–177 (2003)

47. Wedeen, V.J., Hagmann, P., Tseng, W.Y., Reese, T.G., Weisskoff, R.M.: Mapping complex tissue architecture with diffusion spectrum magnetic resonance imaging. Magn. Res. Med. **54**(6), 1377–1386 (2005)
48. Weinstein, D.M., Kindlmann, G.L., Lundberg, E.C.: Tensorlines: Advection-diffusion based propagation through diffusion tensor fields. In: IEEE Visualization, pp. 249–253 (1999)
49. Welk, M., Weickert, J., Becker, F., Schorr, C., Feddern, C., Burgeth, B.: Median and related local filters for tensor-valued images. Signal Process. **87**(2), 291–308 (2007)
50. Westin, C.F., Knutson, H.: Tensor field regularization using normalized convolution. In: Proc. 9th Int. Conf. Computer Aided Systems Theory, pp. 564–572 (2003)
51. Wiegell, M.R., Larsson, H.B., Wedeen, V.J.: Fiber crossing in human brain depicted with diffusion tensor MR imaging. Radiology **217**, 897–903 (2000)
52. Wimberger, D.M., Roberts, T.P., Barkovich, A.J., Prayer, L.M., Moseley, M.E., , Kucharczyk, J.: Identification of premyelination by diffusion-weighted MRI. J. Comp. Assist. Tomogr. **19**(1), 28–33 (1995)
53. Zhukov, L., Barr, A.H.: Oriented tensor reconstruction: Tracing neural pathways from diffusion tensor MRI. In: Proc. IEEE Visualization, pp. 378–394 (2002)
54. Zhukov, L., Barr, A.H.: Heart-muscle fiber reconstruction from diffusion tensor MRI. In: Proc. IEEE Visualization, p. 7984 (2003)